






Lateral solid phase epitaxy of yttrium iron garnet

Sebastian Sailler ^{1,*}, Darius Pohl,² Heike Schlörb,³ Bernd Rellinghaus ², Andy Thomas ^{3,4},
Sebastian T. B. Goennenwein ¹ and Michaela Lammel ^{1,†}

¹Department of Physics, University of Konstanz, 78457 Konstanz, Germany

²Dresden Center for Nanoanalysis (DCN), Dresden, Center for Advancing Electronics Dresden (cfaed),
TUD Dresden University of Technology, 01062 Dresden, Germany

³Leibniz Institute for Solid State and Materials Research Dresden, 01069 Dresden, Germany

⁴Institut für Festkörper- und Materialphysik (IFMP), TUD Dresden University of Technology, 01069 Dresden, Germany



(Received 7 September 2023; accepted 19 January 2024; published 29 February 2024)

Solid phase epitaxy is a crystallization technique used to produce high-quality thin films. Lateral solid phase epitaxy furthermore enables the realization of nonplanar structures, which are interesting, e.g., in the field of spintronics. Here, we demonstrate lateral solid phase epitaxy of yttrium iron garnet over an artificial edge, such that the crystallization direction is perpendicular to the initial seed. We use single-crystalline garnet seed substrates partially covered by a SiO_x film to study the lateral crystallization over the SiO_x mesa. The yttrium iron garnet layer retains the crystal orientation of the substrate not only when in direct contact with the substrate but also across the edge on top of the SiO_x mesa. By controlling the crystallization dynamics it is possible to almost completely suppress the formation of polycrystals and to enable epitaxial growth of single-crystalline yttrium iron garnet on top of mesas made from ceramic materials. From a series of annealing experiments, we extract an activation energy of 3.0 eV and a velocity prefactor of 6.5×10^{14} nm/s for the lateral epitaxial crystallization along the $\langle 100 \rangle$ direction. Our results pave the way to engineer single-crystalline nonplanar yttrium iron garnet structures with controlled crystal orientation.

DOI: [10.1103/PhysRevMaterials.8.L020402](https://doi.org/10.1103/PhysRevMaterials.8.L020402)

Introduction. Epitaxy is one of the most commonly used techniques for obtaining single-crystalline thin films [1,2]. As a subset, solid phase epitaxy (SPE) describes the phase transition of an amorphous solid to its crystalline form while in contact with a crystalline seed of a similar or identical lattice parameter [3]. This causes the crystallization to start from the interface with the seed material and results in a single-crystalline thin film with the same crystal orientation as the seed [3].

A special type of SPE is lateral solid phase epitaxy (LSPE), in which the crystallization direction is perpendicular to the initial seed surface normal [4,5]. Initially, lateral solid phase epitaxy was developed for the fabrication of silicon on insulator structures, and it has been an important technological step for the semiconductor industry [4–7]. Therefore, the SPE of silicon and germanium has been studied most comprehensively [8–11]. Recently, the lateral crystallization of oxide thin films has gained increasing interest and has been shown for Ba_{0.6}Sr_{0.4}TiO₃ [12], Nb : TiO₂ [13], and SrTiO₃ [14].

In this paper we investigate the oxide compound yttrium iron garnet (Y₃Fe₅O₁₂, YIG). Its ferrimagnetic properties [15], combined with a long spin diffusion length [16,17] as well as an exceptionally low Gilbert damping and a low coercive field [18,19], make it a prototypical material in the field of magnetism and spintronics [20].

For typical spintronic experiments, high-quality YIG thin films are needed, as the magnetic and structural properties are connected [18,21]. Over the last approximately 50 years, a multitude of publications on a variety of deposition techniques have shown that getting single-crystalline YIG thin films with excellent quality on lattice-matched substrates such as gadolinium gallium garnet is, indeed, possible [18,19,22–26]. Recently, the exact crystallization dynamics from the amorphous phase on these substrates was reported [27]. However, up to now the literature has almost exclusively described the vertical crystallization (crystallization along the film surface normal) of YIG thin films on a fully coated substrate [18,19,22–26], and the few existing reports using a different approach do not give details concerning the dynamics of the lateral crystallization [28,29]. In this work, we quantitatively analyze the lateral solid phase epitaxy of YIG over an artificial mesa on top of crystalline seed substrates. From systematic annealing experiments we extract the activation energy as well as the crystallization velocity, which allow for a full description of the lateral solid phase epitaxy. Apart from being interesting from a material science point of view, the lateral approach described here opens two interesting avenues. First, it is a key step towards the development of freestanding and easily detachable single-crystalline YIG layers, which can be used in experiments that are otherwise impeded by the substrate materials [30–32]. Second, the possibility to realize epitaxial nonplanar YIG layers facilitates novel experimental solutions to implement, for

*sebastian.sailler@uni-konstanz.de

†michaela.lammel@uni-konstanz.de

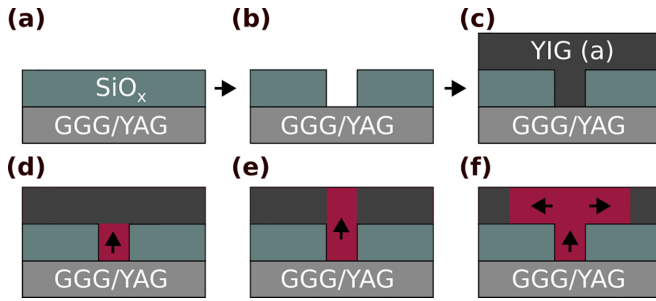


FIG. 1. Sample preparation scheme for lateral crystallization. (a) After coating the single-crystalline substrate with SiO_x , (b) a 1 mm wide trench in the SiO_x is defined by optical lithography and subsequent etching. (c) YIG is afterwards sputtered on top and annealed at 600–650 °C, which induces (d) the crystallization at the substrate interface. (e) After vertically crystallizing, (f) the crystallization front propagates laterally, over the edge of the SiO_x mesa.

example, nonplanar magnon transport and wave computing interconnects [31,33–36].

Methods. All films discussed in this paper were deposited using radio-frequency magnetron sputtering at room temperature in an AJA International sputtering system.

For the lateral crystallization experiments, we used yttrium aluminum garnet ($\text{Y}_3\text{Al}_5\text{O}_{12}$, YAG, CrysTec) substrates with the $\langle 111 \rangle$ crystal orientation being parallel to the surface normal, as well as two types of gadolinium gallium garnet ($\text{Gd}_3\text{Ga}_5\text{O}_{12}$, GGG, SurfaceNet) substrates, for which the crystal orientation along the surface normal is either $\langle 111 \rangle$ or $\langle 001 \rangle$. Since GGG and YAG crystallize in the same space group, $Ia\bar{3}d$, as YIG and their lattice parameters are comparable to those of YIG ($a_{\text{GGG}} = 1.2376$ nm [37], $a_{\text{YAG}} = 1.2009$ nm [37], $a_{\text{YIG}} = 1.2380$ nm [37]), they are considered to be closely lattice matched. Before the sputtering process all substrates were cleaned for 5 mins in acetone and isopropanol and 1 min in deionized water in an ultrasonic bath.

To create an artificial mesa on the substrate surface, we first sputter a nominally 20 nm thick SiO_x layer either from a SiO_2 sinter target or by reactive sputtering from a silicon target onto one of the garnet substrates [see Fig. 1(a)]. The SiO_x layer from the SiO_2 target (reactive Si) was deposited at a sputtering pressure of 2.7×10^{-3} mbar in pure argon atmosphere (argon to oxygen 13:4) at 150 W (100 W) at a rate of 0.0208 nm/s (0.0172 nm/s).

Several methods were utilized to fabricate the mesa from the SiO_x layer [see Fig. 1(b)]. Some of the substrates were partially covered with Kapton tape before the SiO_x sputtering process, which yields the desired structure by simply removing the tape afterwards. While this path is simple, it leads to comparably rough edges. To improve the edge quality of the SiO_x mesa optical lithography and subsequent etching of the SiO_x were utilized. The form of the mesa was first defined in photoresist by a Smart Print (Smartforce Technologies) and, after developing, was transferred into the SiO_x by physical etching with a SF_6 plasma in an Oxford Instrument RIE system. To counteract any potential damage to the substrate after the etching step, it was annealed at 700 °C for 4 h. We also used chemical etching of the SiO_x stripe in buffered HF.

In a subsequent fabrication step, we then deposit the YIG film on top of the predefined SiO_x mesas as sketched in Fig. 1(c). As we want to investigate lateral crystallization, the nominal YIG thickness was chosen to be at least twice as thick as the SiO_x to ensure continuity of the YIG layer across the mesa edge. YIG was sputtered from a stoichiometric sinter target at 2.7×10^{-3} mbar argon pressure and 80 W power at a rate of 0.0135 nm/s. This results in a complete coverage of the SiO_x mesas with YIG, where the YIG film within the predefined trench is still in contact with the lattice-matched substrate [see Fig. 1(c)].

To induce and observe crystallization of the YIG layer, the complete stack was then annealed at temperatures between 600 and 650 °C multiple times in a tube furnace under air. The expected crystallization behavior upon annealing is shown in Figs. 1(d)–1(f). First, YIG starts crystallizing vertically from the lattice-matched substrate via solid phase epitaxy [see Fig. 1(d)]. After reaching the top edge of the film, the epitaxial, single-crystalline YIG now acts as a seed for the amorphous YIG on SiO_x [see Fig. 1(e)]. Starting from the edge of the mesa a lateral crystallization front is expected to move with a constant velocity [see Fig. 1(f)]. The evolution of crystalline YIG across the mesa was observed in a scanning electron microscope (SEM, Zeiss GeminiSEM), where the crystalline region was analyzed via electron backscatter diffraction (EBSD).

Transmission electron microscopy was conducted using a JEOL JEM F200 operated at 200 kV acceleration voltage equipped with a GATAN OneView CMOS camera for fast imaging.

Results and discussion. The selection of the ideal annealing temperature is crucial for the observation of lateral crystallization. In our previous work [27] we determined the parameters describing the vertical crystallization of YIG for different time and temperature pairs depending on the substrate. We demonstrated that epitaxial crystallization from a lattice-matched seed becomes possible at temperatures below those required for the formation of polycrystals. Conversely, the formation of polycrystalline YIG can be suppressed by using sufficiently low annealing temperatures. From our results we approximated that for $T < 660$ °C the formation of a fully polycrystalline film on SiO_x would take about 100 h. Avoiding the formation of polycrystalline grains is of great importance, as those would hinder the epitaxial crystallization. Note that nucleation is a thermally activated process and therefore statistically also possible for lower temperatures. During our study we found that nucleation was more likely to occur if there were external nucleation sites in the form of particles on the respective sample, demonstrating the need for clean surfaces. However, the temperature for annealing has to be sufficiently high since the crystallization rate depends exponentially on the temperature [see Eq. (1)]. Below 540 °C the crystallization via solid phase epitaxy of YIG will not occur in a reasonable amount of time ($t > 100$ h). Therefore, we are confined to a temperature range of about 120 °C (540–660 °C) to study the lateral crystallization of YIG.

To mathematically describe the lateral solid phase epitaxy of YIG from a YIG seed we use a modified Arrhenius equation, which is commonly used for the description of

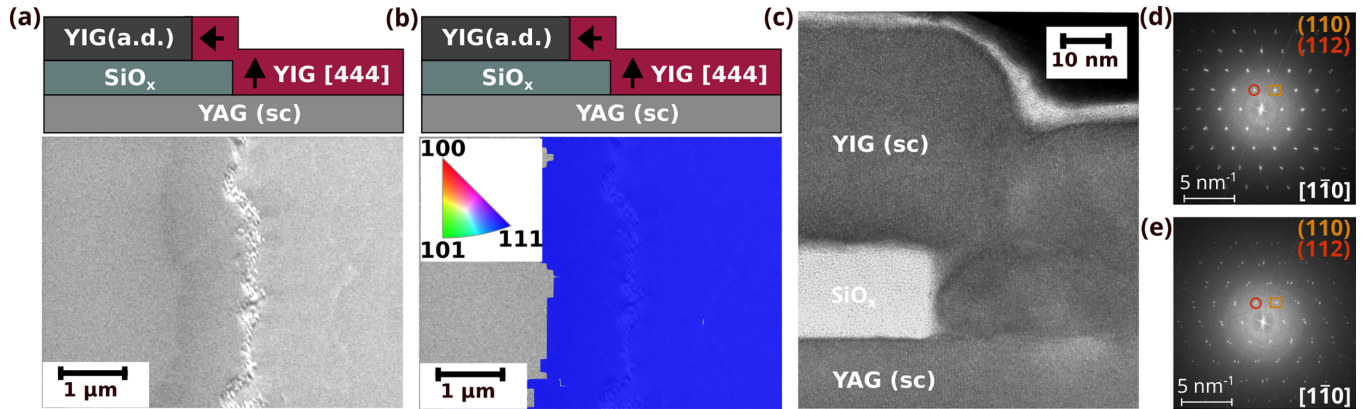


FIG. 2. Observation of lateral crystallization of YIG on a patterned YAG/SiO_x substrate after annealing for 96 h at 600 °C. (a) Secondary electron (SE) image of the mesa etched into the SiO_x, where the left side is elevated as sketched. First, the YIG layer on top of the YAG substrate crystallizes vertically towards the top of the sample and thereby changes from the as-deposited state (a.d.) into a single-crystalline (sc) YIG (right side of the image). Once the YIG reaches the top edge of the sample, it crystallizes laterally via LSPE from right to left onto the SiO_x layer. The formation of crystalline YIG is accompanied by a change in contrast. (b) Superimposing the SE image from (a) with the EBSD mapping confirms the single-crystalline nature of the YIG layer also in the lateral crystallization regime. The color code is taken from the inverse pole figure in the out-of-plane direction and confirms the epitaxial growth in the crystal direction given by the substrate. The TEM investigation in (c) further verifies the lateral solid phase epitaxy of YIG on top of the SiO_x. Directly next to the sharp edge of the SiO_x mesa a slight rotation in the YIG crystal orientation can be seen, which transfers to the single-crystalline YIG on top of the SiO_x, as it grows epitaxially from the YIG seed. To visualize this rotation, the fast Fourier transforms of two TEM images of YIG crystallized laterally on a SiO_x mesa, one near the mesa edge and one near the end of the crystallization front, are depicted in (d) and (e), respectively. Here, the zone axis is along [110], and two reflections along (110) and (112) are marked.

homoepitaxial crystallization out of the amorphous phase [3,11,38,39]. This description assumes a homogeneous crystallization front that moves through an amorphous material starting from a crystalline seed of the same material. At a given temperature T , this crystallization front is expected to move with a constant velocity ($v = \frac{l}{t}$). Here, v is the lateral crystallization velocity, l is the lateral crystallization distance, and t is the annealing time. The crystallization velocity itself depends exponentially on the temperature as well as the activation energy E_A and can be described by [3,38]

$$v = v_0 \cdot e^{\frac{-E_A}{k_B T}}, \quad (1)$$

where k_B is the Boltzmann constant and the prefactor v_0 represents a maximal velocity.

To confirm LSPE of YIG and to determine the crystallization velocities $v(T)$, we analyze our samples with EBSD for a sequence of annealing times. EBSD also allows us to exclude polycrystalline YIG on top of the SiO_x mesa. A secondary electron (SE) image taken across the edge of the mesa is depicted in Fig. 2(a). On the right, crystalline YIG is on top of the YAG substrate as depicted in the schematics above the SE image. The lateral crystallization front moves from the right across the mesa's edge, which can be seen in the middle of the image, towards the left. The area of crystallized YIG on top of the SiO_x mesa can be discerned as a change in gray level, which we ascribe to the height and density change upon crystallization.

To verify the formation of single-crystalline YIG on YAG as well as across the mesa on SiO_x, the SE image is superimposed with the results from the EBSD mapping [see Fig. 2(b)]. The monochrome color of the inverse pole figure from the out-of-plane direction confirms an epitaxial

formation of single-crystalline YIG initiated by the substrate. This demonstrates that we achieved lateral solid phase epitaxy of 1 μm YIG over a 18 nm high mesa. Furthermore, unlike in similar studies on Si and other oxides [4,5,13,14], we do not find any polycrystalline YIG seeds on SiO_x after 96 h at 600 °C.

To further investigate the single-crystalline nature of the laterally crystallized YIG, transmission electron microscopy (TEM) was performed. Figure 2(c) depicts a side view of the mesa structure as illustrated schematically in Figs. 1(f), 2(a), and 2(b). The TEM images show a sharp edge of the deposited SiO_x and a rounder YIG edge on top [Fig. 2(c)]. On top of the YIG a conducting layer consisting of Au/Pd/Pt was utilized, which prevents amorphization of the otherwise isolating sample by the ion beam due to charging effects. The TEM image supports the results of the SEM investigation in that the YIG layer crystallizes epitaxially from the substrate and also laterally on top of the SiO_x layer. However, close to the SiO_x edge in Fig. 2(c), some imperfections in the single crystal can be resolved in the TEM image. Additionally, a rotation of the crystal is visible. A tilted YIG crystallizing from the bottom acts as the new seed for the lateral crystallization and therefore causes the YIG crystal on top of the SiO_x to be slightly rotated with respect to the substrate. As this rotation takes place over an extended distance, it is not prevalent in Fig. 2(c). To visualize the rotation we include the fast Fourier transforms (FFTs) obtained from two TEM images: one near the mesa edge [see Fig. 2(d)] and one at the end of the crystallization front [see Fig. 2(e)]. In the FFTs, a clear rotation of the YIG peaks is observed. This rotation is visible in samples in which the surface normal is parallel to the [111] direction but not in samples with the surface normal direction parallel to [100]. Additionally, the rotation

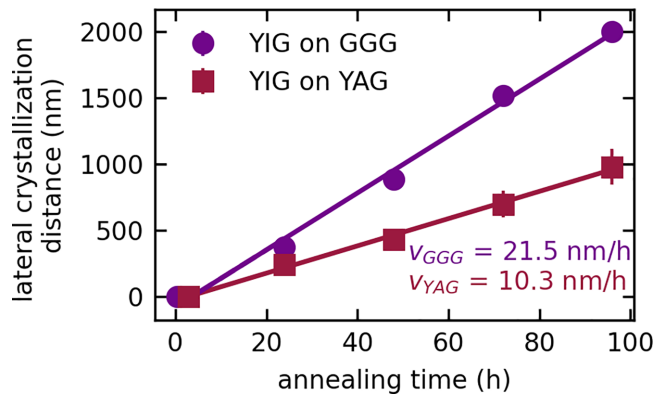


FIG. 3. Lateral crystallization velocities for YIG at 600°C on two different seed substrates. After the sample was annealed for 24 h the lateral crystallization distance was extracted from multiple SEM images of different areas over the mesa edge, and the sample was annealed again. The average lateral crystallization with the standard deviation is depicted over the annealing time. A linear fit to the data was used to extract the lateral crystallization rate and the delay before the onset of lateral crystallization. While YIG starts to grow earlier on YAG, it shows a slower rate of 10.3 nm/h compared to the 21.5 nm/h on GGG.

takes place exclusively in planes perpendicular to the $[1\bar{1}0]$ direction of YIG.

The distance up to which the YIG crystallizes laterally on top of the SiO_x can be extracted from both techniques, TEM and scanning electron microscopy. As the SEM allows for a fast measurement of the crystallization front, the lateral crystallization data are extracted from the SE images and EBSD data.

To determine the lateral crystallization velocities, each sample is annealed multiple times and the distance covered by the crystallization front is measured after each annealing step. At each time and temperature pair we analyze multiple images across the mesa edge and thereby obtain the respective average crystallization distance and its standard deviation. The time which corresponds to a lateral crystallization distance of 0 nm is approximated by the time necessary for the YIG to crystallize vertically up to the height of the step, e.g., 0.34 h for a step height of 20 nm with a vertical crystallization velocity of 58.8 nm/h for YIG on GGG at 600°C, as detailed in our previous work [27]. We then determine the lateral crystallization velocity from the slope of a linear fit to the data.

Figure 3 shows the lateral crystallization velocity of YIG at 600°C when using $\langle 111 \rangle$ -oriented YAG and GGG as seed substrates. We extract a lateral crystallization velocity of $v_{\text{YAG}} = 10.3$ nm/h (0.003 nm/s) for YIG on YAG and $v_{\text{GGG}} = 21.5$ nm/h (0.006 nm/s) for YIG on GGG.

Since the lateral crystallization starts from a YIG seed for either of the substrates, one might expect the same lateral crystallization velocity. However, the different velocities suggest that the substrate indeed influences the maximal crystallization velocity. On the one hand, this behavior might originate from different crystalline qualities of the vertically crystallized YIG on the two substrates. Since GGG exhibits a lower lattice mismatch than YAG, it is expected to lead to a higher-quality YIG film from epitaxy. On the other hand, the

crystallization was not perfectly epitaxial near the SiO_x mesa [see Fig. 2(c)], which could influence the initial crystallization as well as the final velocity. In the course of this work we observed that the final velocity depends on the surface and mesa edge quality.

To further substantiate our results, we compare our lateral crystallization velocity to the vertical crystallization velocity of YIG, which we reported in an earlier work [27]. Compared to the vertical crystallization velocity of 58.8 nm/h (0.016 nm/s) for a YIG thin film on GGG, the lateral crystallization velocity of YIG on GGG v_{GGG} is 3.6 times slower. A similar trend is seen on YAG, where the lateral crystallization velocity v_{YAG} is roughly 1.6 times slower than the vertical crystallization velocity of YIG on YAG of 16.2 nm/h (0.0045 nm/s). We speculate that the YIG crystal quality impacts the crystallization speed, but more detailed experiments will be necessary to resolve this point in the future. Since the vertical crystallization of YIG on GGG was confirmed to be epitaxial, it allows for a good comparison with the LSPE of YIG. The observation that the lateral crystallization is slower than the vertical one is naively unexpected but was also reported for silicon, where the lateral crystallization was 4 to 8 times slower than that in the vertical direction [4]. In silicon this behavior was ascribed to the formation of facets and defects in the lateral silicon.

Another reason for the slower lateral crystallization velocity could be a dependence on the crystal direction along which the YIG crystallizes. From studies on silicon it is known that differences in vertical crystallization velocity [8,9] are transferred to the lateral crystallization [6]. Such a crystal orientation dependence of the crystallization velocities was also reported for bulk YIG [40–42].

Hence, to compare the lateral crystallization velocities extracted here with the ones from our previous work that describe the vertical crystallization, the direction along which the crystallization takes place needs to be taken into account [43]. Together with the different seed substrates, this direction dependence could play a role in the difference of a factor of 3.6 between the lateral crystallization velocity and the vertical one for YIG on GGG.

In addition to the possibility of direction dependence the lateral solid phase epitaxy of YIG is expected to exponentially depend on the temperature as described in Eq. (1).

To investigate both the crystal orientation dependence and the temperature dependence, multiple samples were prepared on GGG substrates with the $[001]$ and $[111]$ directions parallel to the surface normal. These orientations allow for the investigation of the lateral crystallization velocity along the $[010]$, $[100]$, $[1\bar{1}0]$, and $[11\bar{2}]$ directions. As YIG is a cubic system, these will be referred to by their equivalents, $\langle 100 \rangle$, $\langle 110 \rangle$, and $\langle 112 \rangle$. The crystallization along these directions was evaluated for samples annealed at different temperatures of 600, 625, 637, and 650°C.

Although the formation of some polycrystalline grains could be seen with increasing temperature, that did not hinder the lateral crystallization up to a distance of 2.2 μm via LSPE. This distance results from our choice of maximum annealing time at each tested temperature. Note that while, in principle, the lateral crystallization should continue through the whole layer, for very long times and/or higher annealing

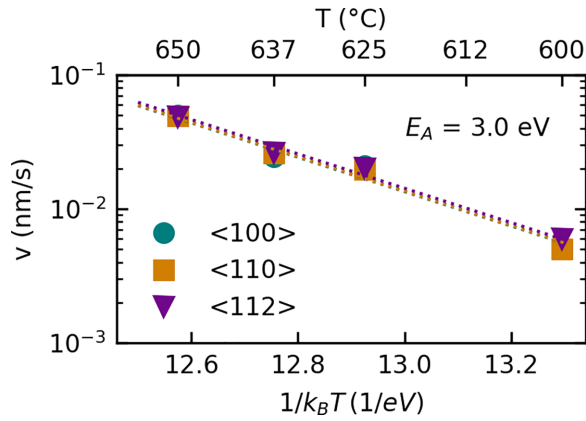


FIG. 4. Crystallization velocities as a function of temperature along different crystal directions on a GGG substrate. A semilogarithmic plot over the inverse temperature yields the activation energy E_A as well as the maximal rates v_0 . For YIG an activation energy of $E_A = 3.0$ eV is found. The crystallization velocity depends only marginally on the direction and is $v_0(\langle 100 \rangle) = 6.5 \times 10^{14}$ nm/s, $v_0(\langle 110 \rangle) = 6.5 \times 10^{14}$ nm/s, and $v_0(\langle 112 \rangle) = 6.9 \times 10^{14}$ nm/s.

temperatures the statistical formation of grains can impede the propagation of the crystallization front.

Figure 4 shows the results of these series over the annealing temperature. Each velocity shown in Fig. 4 is extracted from a series like the one shown in Fig. 3. From the semilogarithmic plot, the linear dependence of the lateral crystallization velocity on the inverse temperature can be seen. Here, the lateral crystallization velocity increases from 21.5 nm/h (0.006 nm/s) at 600 °C up to 173.1 nm/h (0.048 nm/s) at 650 °C. As all the samples are made of the same material, i.e., YIG, we expect one single activation energy for all directions [9–11,38,44], which we extract from the slope of a linear fit to all velocities. This results in an activation energy of $E_A = 3.0 \pm 0.2$ eV for the lateral crystallization of YIG.

In contrast to the reports for the formation of bulk YIG [42], however, we find no significant difference in the maximal lateral crystallization velocity depending on crystal orientation. For the formation of bulk YIG from the liquid phase it was reported that facets in the $\langle 110 \rangle$ and $\langle 112 \rangle$ directions are the thermodynamically most stable, while the $\langle 111 \rangle$ direction was described to grow the fastest [41,42,45]. There, YIG was found to crystallize up to 10 times faster along the $\langle 111 \rangle$ direction than along the $\langle 110 \rangle$ direction [41], while the crystallization velocities along the $\langle 110 \rangle$ and $\langle 112 \rangle$ directions were found to behave very similarly [42].

For the LSPE of our sputtered thin films with an activation energy of 3.0 eV we find prefactors of $v_0(\langle 100 \rangle) = 6.5 \times 10^{14}$ nm/s, $v_0(\langle 110 \rangle) = 6.5 \times 10^{14}$ nm/s, and $v_0(\langle 112 \rangle) = 6.9 \times 10^{14}$ nm/s. Tolsdorf and Bartels reported a very similar growth behavior of YIG grown by liquid phase epitaxy for facets along the $\langle 110 \rangle$ and $\langle 112 \rangle$ directions, with the $\langle 112 \rangle$ direction being slightly faster, which we find here as well [42]. No qualitative literature data could be found for the crystallization along the $\langle 100 \rangle$ direction. Further studies involving lateral growth along the faster crystallizing $\langle 111 \rangle$ direction [41,42] could help to verify the orientation dependence of lateral YIG growth.

TABLE I. Activation energies E_A and prefactors v_0 of the epitaxial YIG from our work in comparison with silicon, germanium, and SrTiO₃.

Material	Ref.	Orientation	E_A (eV)	v_0 (nm/s)
YIG	this work	$\langle 100 \rangle$	3.0 ± 0.2	6.5×10^{14}
YIG	this work	$\langle 110 \rangle$	3.0 ± 0.2	6.5×10^{14}
YIG	this work	$\langle 112 \rangle$	3.0 ± 0.2	6.9×10^{14}
Si	Csepregi <i>et al.</i> [38]	$\langle 100 \rangle$	2.3 ± 0.1	1.5×10^{13}
Si	Csepregi <i>et al.</i> [38]	$\langle 110 \rangle$	2.3 ± 0.1	6.4×10^{12}
Ge	Johnson <i>et al.</i> [11]	$\langle 100 \rangle$	2.15 ± 0.04	2.6×10^{16}
SrTiO ₃	White <i>et al.</i> [39]	$\langle 100 \rangle$	0.77	5×10^5
SrTiO ₃	Chen <i>et al.</i> [46]	$\langle 100 \rangle$	0.7	7.8×10^2

Both the activation energies E_A and the prefactors v_0 are in good agreement with the literature for solid phase epitaxy (see Table I). Compared to the model systems of silicon, germanium, and SrTiO₃, the activation energy for YIG is higher, while the crystallization velocities are of a similar order of magnitude as for silicon and germanium. The epitaxial crystallization process of YIG seems to be more similar to that of elemental Si and Ge than to that of the oxide SrTiO₃.

Additionally, our activation energy of $E_A = 3.0$ eV \pm 0.2 eV for epitaxial YIG compares well with previously reported values. Specifically, investigations of YIG thin films on GGG revealed an activation energy of 3.98 eV [27]. This increased activation energy on a not perfectly lattice matched substrate can be seen as the additional barrier that needs to be overcome to start the crystallization process. For the formation of bulk, polycrystalline YIG from oxide powders, a value of 5.08 eV was reported [47]. Chen *et al.* [46] reported that the activation energy for epitaxial SrTiO₃ is half of that of polycrystalline SrTiO₃, which is in good agreement with our findings for the YIG thin films. The activation energy for solid phase epitaxy of $E_A = 3.0$ eV is also roughly half of 5.08 eV for the oxide powders and also reduced compared to the value of vertical crystallization on GGG substrates. We therefore conclude that the lateral solid phase epitaxy of YIG is described by an activation energy of $E_A = 3.0$ eV and, for the directions $\langle 100 \rangle$, $\langle 110 \rangle$, and $\langle 112 \rangle$, by v_0 values of 6.5×10^{14} , 6.5×10^{14} and 6.9×10^{14} nm/s, respectively.

Conclusion. To assess the lateral solid phase epitaxy of YIG, we defined SiO_x mesa structures on top of single-crystalline garnet substrates, which were subsequently covered by an amorphous YIG layer by room temperature sputtering. By carefully choosing the annealing temperature we were able to laterally crystallize up to 2.2 μ m of single-crystalline YIG on top of an amorphous SiO_x layer. At 600 °C on GGG a crystallization velocity of 21.5 nm/h (0.006 nm/s) was found, which increased by a factor of 7 to 173.1 nm/h (0.048 nm/s) at 650 °C. By extracting multiple lateral crystallization velocities at different temperatures and along different crystal orientations, we confirmed an exponential dependence on temperature as expected for LSPE. The resulting crystallization parameters are summarized in Table I, where the crystallization velocity we derived is mostly independent of the crystal orientation of the seed. The understanding of these dynamics allows for a controlled and precise manufacturing of single-crystalline

YIG thin films of micrometer length scales on various substrates.

Acknowledgments. This work was funded by the Deutsche Forschungsgemeinschaft (DFG, German Research Foundation), Project ID No. 446571927, and via the SFB 1432,

Project ID No. 425217212. We gratefully acknowledge technical support and advice from the nano.lab facility of the University Konstanz. We acknowledge the use of the facilities in the Dresden Center for Nanoanalysis (DCN) at Technische Universität Dresden and the support of A. Tahn.

-
- [1] G. B. Stringfellow, *Rep. Prog. Phys.* **45**, 469 (1982).
- [2] P. G. Evans, Y. Chen, J. A. Tilka, S. E. Babcock, and T. F. Kuech, *Curr. Opin. Solid State Mater. Sci.* **22**, 229 (2018).
- [3] B. C. Johnson, J. C. McCallum, and M. J. Aziz, *Handbook of Crystal Growth* (Elsevier North-Holland, Boston, 2015), pp. 317–363.
- [4] H. Ishiwara, H. Yamamoto, S. Furukawa, M. Tamura, and T. Tokuyama, *Appl. Phys. Lett.* **43**, 1028 (1983).
- [5] H. Ishiwara, M. Tanaka, and S. Furukawa, *Appl. Phys. Lett.* **49**, 1363 (1986).
- [6] K. Kusakawa, M. Moniwa, M. Ohkura, and E. Takeda, *Appl. Phys. Lett.* **56**, 560 (1990).
- [7] B. Hoefflinger, in *Chips 2020*, edited by B. Hoefflinger, The Frontiers Collection (Springer, Berlin, 2011), pp. 161–174.
- [8] L. Csepregi, J. W. Mayer, and T. W. Sigmon, *Appl. Phys. Lett.* **29**, 92 (1976).
- [9] L. Csepregi, R. Küllen, J. Mayer, and T. Sigmon, *Solid State Commun.* **21**, 1019 (1977).
- [10] J. S. Williams, *Nucl. Instrum. Methods Phys. Res.* **209–210**, 219 (1983).
- [11] B. C. Johnson, P. Gortmaker, and J. C. McCallum, *Phys. Rev. B* **77**, 214109 (2008).
- [12] J.-S. Lee and S.-K. Joo, *Jpn. J. Appl. Phys.* **39**, 6343 (2000).
- [13] K. Taira, Y. Hirose, S. Nakao, N. Yamada, T. Kogure, T. Shibata, T. Sasaki, and T. Hasegawa, *ACS Nano* **8**, 6145 (2014).
- [14] Y. Chen, J. A. Tilka, Y. Ahn, J. Park, A. Pateras, T. Zhou, D. E. Savage, I. McNulty, M. V. Holt, D. M. Paskiewicz, D. D. Fong, T. F. Kuech, and P. G. Evans, *J. Phys. Chem. C* **123**, 7447 (2019).
- [15] M. Althammer, S. Meyer, H. Nakayama, M. Schreier, S. Altmannshofer, M. Weiler, H. Huebl, S. Geprägs, M. Opel, R. Gross, D. Meier, C. Klewe, T. Kuschel, J.-M. Schmalhorst, G. Reiss, L. Shen, A. Gupta, Y.-T. Chen, G. E. W. Bauer, E. Saitoh, and S. T. B. Goennenwein, *Phys. Rev. B* **87**, 224401 (2013).
- [16] Y. Kajiwara, K. Harii, S. Takahashi, J. Ohe, K. Uchida, M. Mizuguchi, H. Umezawa, H. Kawai, K. Ando, K. Takanashi, S. Maekawa, and E. Saitoh, *Nature (London)* **464**, 262 (2010).
- [17] L. Cornelissen, J. Liu, R. Duine, J. B. Youssef, and B. Van Wees, *Nat. Phys.* **11**, 1022 (2015).
- [18] H. Chang, P. Li, W. Zhang, T. Liu, A. Hoffmann, L. Deng, and M. Wu, *IEEE Magn. Lett.* **5**, 1 (2014).
- [19] C. Hauser, T. Richter, N. Homonnay, C. Eisenschmidt, M. Qaid, H. Deniz, D. Hesse, M. Sawicki, S. Ebbinghaus, and G. Schmidt, *Sci. Rep.* **6**, 20827 (2016).
- [20] V. Cherepanov, I. Kolokolov, and V. L'vov, *Phys. Rep.* **229**, 81 (1993).
- [21] M. Haidar, M. Ranjbar, M. Balinsky, R. K. Dumas, S. Khartsev, and J. Åkerman, *J. Appl. Phys.* **117**, 17D119 (2015).
- [22] N. Beaulieu, N. Kervarec, N. Thiery, O. Klein, V. Naletov, H. Hurdequint, G. De Loubens, J. B. Youssef, and N. Vukadinovic, *IEEE Magn. Lett.* **9**, 1 (2018).
- [23] C. Dubs, O. Surzhenko, R. Thomas, J. Osten, T. Schneider, K. Lenz, J. Grenzer, R. Hübner, and E. Wendler, *Phys. Rev. Mater.* **4**, 024416 (2020).
- [24] Y. Krockenberger, H. Matsui, T. Hasegawa, M. Kawasaki, and Y. Tokura, *Appl. Phys. Lett.* **93**, 092505 (2008).
- [25] P. W. Jang and J. Y. Kim, *IEEE Trans. Magn.* **37**, 2438 (2001).
- [26] M. Lammel, D. Scheffler, D. Pohl, P. Swekis, S. Reitzig, S. Piontek, H. Reichlova, R. Schlitz, K. Geishendorf, L. Siegl, B. Rellinghaus, L. M. Eng, K. Nielsch, S. T. B. Goennenwein, and A. Thomas, *Phys. Rev. Mater.* **6**, 044411 (2022).
- [27] S. Sailer, G. Skobjin, H. Schlörb, B. Boehm, O. Hellwig, A. Thomas, S. T. B. Goennenwein, and M. Lammel, *arXiv:2308.00412* [Phys. Rev. Mater. (to be published)].
- [28] F. Heyroth, C. Hauser, P. Trempler, P. Geyer, F. Syrowatka, R. Dreyer, S. G. Ebbinghaus, G. Woltersdorf, and G. Schmidt, *Phys. Rev. Appl.* **12**, 054031 (2019).
- [29] Heyroth *et al.* [28] showcased a single-crystalline YIG bridge fabricated by coating a resist template with YIG deposited via pulsed laser deposition. However, we do not expect their annealing process to be easily transferrable to larger, sputtered YIG structures, as we see significant formation of polycrystalline YIG above.
- [30] S. Kosen, A. F. Van Loo, D. A. Bozhko, L. Mihalceanu, and A. D. Karenowska, *APL Mater.* **7**, 101120 (2019).
- [31] A. Barman *et al.*, *J. Phys.: Condens. Matter* **33**, 413001 (2021).
- [32] S. Guo, B. McCullian, P. Chris Hammel, and F. Yang, *J. Magn. Mater.* **562**, 169795 (2022).
- [33] A. V. Chumak, V. Vasyuchka, A. Serga, and B. Hillebrands, *Nat. Phys.* **11**, 453 (2015).
- [34] V. K. Sakharov, E. N. Beginin, Y. V. Khivintsev, A. V. Sadovnikov, A. I. Stognij, Y. A. Filimonov, and S. A. Nikitov, *Appl. Phys. Lett.* **117**, 022403 (2020).
- [35] M. M. Salazar-Cardona, L. Körber, H. Schultheiss, K. Lenz, A. Thomas, K. Nielsch, A. Kákay, and J. A. Otálora, *Appl. Phys. Lett.* **118**, 262411 (2021).
- [36] A. V. Chumak *et al.*, *IEEE Trans. Magn.* **58**, 1 (2022).
- [37] S. Gates-Rector and T. Blanton, *Powder Diffr.* **34**, 352 (2019).
- [38] L. Csepregi, J. Mayer, and T. Sigmon, *Phys. Lett. A* **54**, 157 (1975).
- [39] C. White, L. Boatner, P. Sklad, C. McHargue, J. Rankin, G. Farlow, and M. Aziz, *Nucl. Instrum. Methods Phys. Res., Sect. B* **32**, 11 (1988).
- [40] J. W. Nielsen and E. F. Dearborn, *J. Phys. Chem. Solids* **5**, 202 (1958).
- [41] W. V. Erk, H. J. G. J. Van Hoek-Martens, and G. Bartels, *J. Cryst. Growth* **48**, 621 (1980).

- [42] W. Tolksdorf and I. Bartels, *J. Cryst. Growth* **54**, 417 (1981).
- [43] The direction of the lateral crystallization of the YIG layers from Fig. 3 can be identified as $[11\bar{2}]$, as it is perpendicular to $[111]$ and $[1\bar{1}0]$ known from the substrate. There, the $[111]$ direction is parallel to the surface normal of the substrate, which is cut in a way to have one edge aligned parallel to the $[1\bar{1}0]$ direction. The vertical crystallization on GGG took place along the $[111]$ direction [27].
- [44] A. Claverie, S. Koffel, N. Cherkashin, G. Benassayag, and P. Scheiblin, *Thin Solid Films* **518**, 2307 (2010).
- [45] E. Beregi, E. Sterk, F. Tanos, E. Hartmann, and J. Lábár, *J. Cryst. Growth* **65**, 562 (1983).
- [46] Y. Chen, M. H. Yusuf, Y. Guan, R. Jacobson, M. G. Lagally, S. E. Babcock, T. F. Kuech, and P. G. Evans, *ACS Appl. Mater. Interfaces* **9**, 41034 (2017).
- [47] W. F. F. Wan Ali, M. Othman, M. F. Ain, N. S. Abdullah, and Z. A. Ahmad, *J. Am. Ceram. Soc.* **99**, 315 (2016).